*Sensors and Materials,* Vol. 21, No. 3 (2009) 167–177
MYU Tokyo

S & M 0757

# Proposal of a Double-Gate Split-Drain/Source MAGFET with Bulk Conduction in FD SOI Technology

Nebojsa D. Jankovic

Faculty of Electronic Engineering Nis, University of Nis,
Aleksandra Medvedeva 14, 18000 Nis, Serbia

(Received October 28, 2008; accepted February 10, 2009)

***Key words:*** magnetic, sensor, MAGFET, SOI, fully depleted

In this paper, the design and operation of a double-gate split-drain/source magnetic field-effect transistor (DG SDS MAGFET) compatible with fully depleted (FD) thin-film silicon-on-isolator (SOI) technology are described. Owing to bulk conduction and carrier-domain-based operation of a DG SDS MAGFET, a magnetic sensitivity of 58 $T^{-1}$ in the mT range of magnetic fields is predicted from a three-dimensional sensor numerical simulation. This is almost two orders of magnitude higher than the magnetic sensitivity achieved with conventionally designed MAGFETs in FD SOI technology. In addition, the simulation results revealed that the DG SDS MAGFET can also operate as a bidirectional cross-switch controlled by a pulsed magnetic field with an amplitude above 30 mT.

## 1. Introduction

When a single-drain region of a metal-oxide-semiconductor field-effect transistor (MOSFET) is split into two adjacent regions, the associated drain currents will become sensitive to the magnetic field applied perpendicularly to the device surface. Such a MOSFET is usually called a magnetic field-effect transistor (MAGFET).[1] The integration of MAGFETs together with support and signal processing circuitry on the same silicon chip is being further developed for a variety of applications.[2] Nowadays, integrated magnetic sensors are routinely fabricated with bulk CMOS processing technologies.[3] Recently, a fully depleted (FD) thin-film silicon-on-isolator (SOI) technology has emerged as a major contender for future integrated microsensors and microsystems with the unique advantages that SOI offers in some application niches, such as high-temperature and RF and/or micropower operation.[4,5] Thus, the design of MAGFETs in FD SOI technology has copied the layout of long-gate split-drain MAGFETs originally designed for bulk CMOS technology.[6–8] It is observed that MAGFETs in FD SOI technology have low magnetic sensitivities similar to their bulk

*Corresponding author: e-mail: nebojsa.jankovic@elfak.ni.ac.yu

CMOS counterparts falling in the range of (0.05–1.5) $T^{-1}$.[6–8] This limited magnetic sensitivity of conventionally designed bulk or FD SOI MAGFETs is predominantly caused by the low mobility of their carriers transported through the MOS surface channel, which is known to be more than twofold lower than the mobility of bulk carriers.[3]

A higher sensitivity is always desired since it helps to simplify the system, reduce cost, and decrease power consumption, and may open new applications. For this reason, we will describe in this paper a new double-gate (DG) split-drain/source (SDS) MAGFET compatible with FD SOI technology that has the potential to overcome the aforementioned sensitivity limitations of conventional MAGFETs. The advantages of the DG SDS MAGFET design stems from the particular physics of device internal operation, where charge carrier transport is predominated primarily by a bulk conduction of electrons in fully depleted intrinsic silicon thin films. It will be shown in this paper that, owing to the high mobility of bulk carriers, a substantially higher magnetic sensitivity of DG SDS MAGFETs than that of conventional MAGFETs can be obtained. The electrical and magnetic behaviors of the new sensor device as well as its potential use as a magnetically controlled bidirectional cross-switch will also be discussed in detail using a three-dimensional (3D) device numerical simulator, ATLAS from SILVACO.[9] ATLAS has recently been upgraded to take into account the effect of external magnetic fields on semiconductor devices.

## 2. Device Description and Analysis

### 2.1 *Device description*

The 3D structure of the *n*-channel DG SDS MAGFET studied in this work is shown in Fig. 1. The device design is inspired by a classical double-gate FinFET device in

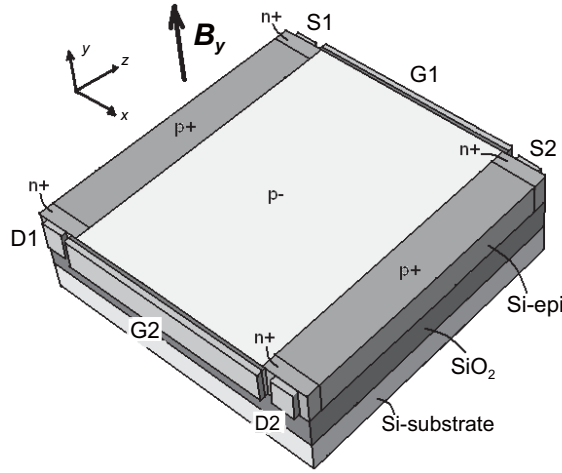


Fig. 1. Three-dimensional view of DG SDS MAGFET in FD SOI technology.

SOI technology originally proposed by Hisamoto *et al*. in 1991 for deep-submicrometer MOSFET design.[10] Thus, similarly to FinFET design, the DG SDS MAGFET structure is a nonplanar, double-gate transistor built on an SOI substrate, where conducting channels exist on both sides of a thin silicon "fin" forming the device body. The device operation can be understood as the parallel connection of two folded-channel FiNFETs with associated groups of electrodes: S1, G1(half), G2(half)D1 and S2, G1(half), G2(half), D2. The electrons injected from S1 (S2) flow in part through the corresponding half of the G1 channel in the *x*-direction; then, they acquire transversal bulk transport in the *z*-direction of the fin's middle area towards G2, until they are collected by the corresponding half of the G2 channel, where they move in the *x*-direction toward the D1 (D2) drain electrode. The two gate electrodes G1 and G2 are assumed to be made of metal with a midgap work function difference $\Phi_{ms} = 4.55$ eV. A $5 \times 5$ μm$^2$ device area, a 1 μm silicon fin body thickness, and a 15 nm gate oxide thickness are adopted as geometrical parameters of the device shown in Fig. 1. The central fin's area representing the channel region has an almost intrinsic p-type doping concentration ($p^- = 5 \times 10^{13}$ cm$^{-3}$), while the two outer $p^+$-doped regions aligned in the *z*-direction to S1, D1 and S2, D2 diffusions are highly doped ($p^+ = 10^{18}$ cm$^{-3}$). As shown in Fig. 1, there are also two identical pairs of $n^+$-doped regions denoted S1, S2 and D1, D2, which form the sources and drains of two parallel FiNFETs, respectively. For simplicity, they are assumed to be uniformly doped ($n^+ = 10^{21}$ cm$^{-3}$) and to have equal junction depths along the *z*-axis (0, 5 μm). Each source and drain pair is ideally self-aligned to its corresponding gate electrode, *e.g.*, S1, S2 with G1 and D1, D2 with G2, as shown in Fig. 1. Note that the threshold voltage $V_{t0}$ required to invert both channels at zero drain-source biasing voltages is estimated for this device to be approximately 0.3 V.

For further reference, the orientation of the three-axis Cartesian coordinate system used in 3D device simulations is also shown in Fig. 1. Its origin is situated in the corner of the device upper surface near the S1 electrode. In addition, the perpendicular magnetic field $\vec{B}_y$ shown in Fig. 1 is assumed positive and negative when it complies and does not comply with the direction of the *y*-axis unity vector, respectively.

## 2.2 *Electrical behavior*

Despite its structural similarities to the FD FiNFET design, the DG SDS MAGFET substantially differs in operation from conventional MOSFETs. To clarify this difference, we employed a 3D device numerical simulation for sensor analysis. The default values of the silicon physical parameters of SILVACO ATLAS[9] software are used for 3D device numerical simulation.

Figure 2 shows the potential and current density distributions of the DG SDS MAGFET that were obtained from device simulations performed for S1, S2-grounded and G1, G2-shorted, and for device biasing at $V_{GS} = 5$ V and $V_{DS} = 3$ V. On the basis of these simulations, we found that the two different modes of DG SDS MAGFET operation can be defined as the "above-threshold" and "subthreshold" modes.

The above-threshold mode appears for $V_{GS} > V_{DS}+V_{t0}$, where both surface channels G1 and G2 are fully inverted. In addition, the $p^-$-doped fin region bounded by the G1 and G2 electrodes is fully depleted in this region, since the potential gradient exists only in

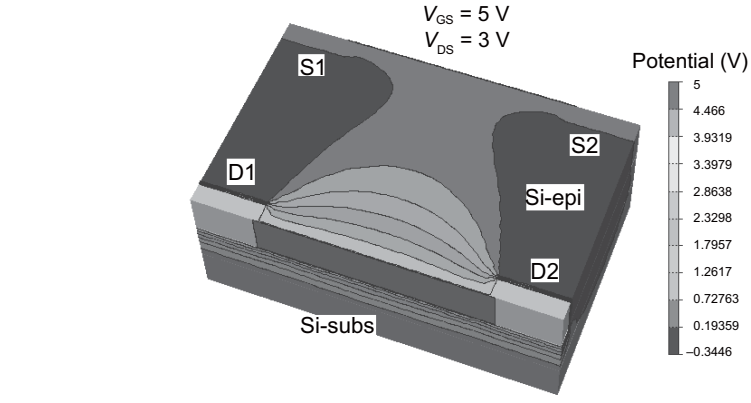


(a)

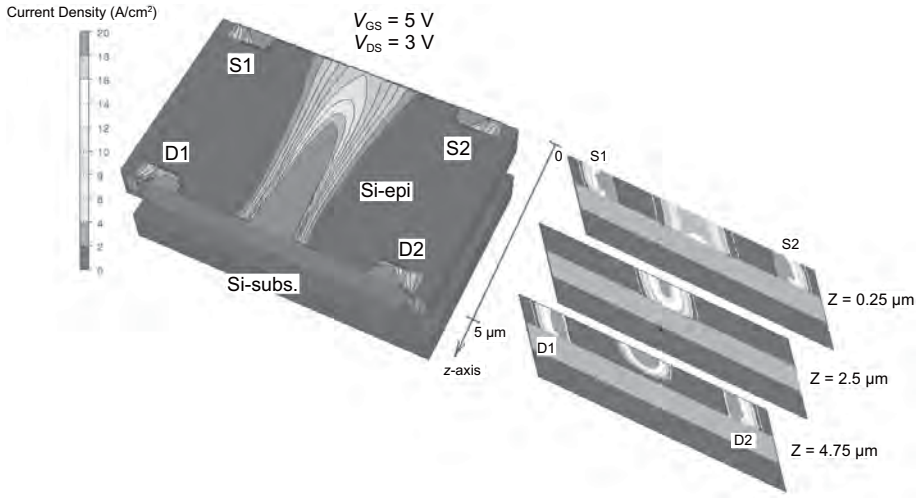


(b)

Fig. 2. Potential and current density distributions of DG SDS MAGFET simulated with ATLAS SILVACO[9] for $V_{GS}$ = 5 V and $V_{DS}$ = 3 V.

the intrinsic fin area shown in Fig. 2(a). Owing to the penetration of the D1 (D2) electric field lines into the G1 channel depletion region, the injection of electrons from the G1 surface channel middle area is initiated; the electrons are subsequently swept by the D1 (D2) drain electric fields toward the opposite G2 channel region. This establishes a substantial transversal electron current flow with bulk conduction in the intrinsic fin area of the DG SDS MAGFET. Figure 2(b) shows that the transversal current flow is concentrated in the narrow region of the fin's middle area, which resembles the operation of so called "carrier domain" magnetic sensors.[11] The "carrier domain"-like current flow is more clearly

observed in associated current density cross sections of the device rendered at $z$ = 0.25, 2.5, and 4.75 μm, as shown in Fig. 2(b). Note that the red area in these cross sections denoting "carrier domains" shrinks while approaching the G2 channel region. This implies that the density of electrons in the transversal electron flux also increases along the $z$-axis from G1 towards G2. To satisfy the current continuity condition, this charge density increase must be followed by a corresponding increase in electron drift velocity. This means that electrons traveling in a fully depleted fin along the $z$-axis rapidly reach their drift saturation velocity, which favors an increase in the magnetic sensitivity of the device, as will be explained in the next subsection.

The second mode of DG SDS MAGFET operation is the subthreshold mode defined as $V_{t0} < V_{GS} < V_{DS}+V_{t0}$. Namely, in this mode of sensor operation, the G1 surface is in a weak inversion state owing to the effects of $V_{DS}$ and $V_{GS}$ acting as a back bias for the G1 channel. In contrast, the surface of the G2 channel is fully inverted, since the S1 (S2) electrodes are maintained at ground potential and they do not affect the G2 channel potential. In the subthreshold mode, however, the potential barriers of the $n^+/p^-$ junctions of the S1 (S2) electrodes are decreased owing to the effects of $V_{GS}$ and $V_{DS}$. Consequently, the bipolar injection of electrons from the $n^+/p^-$ junctions of the S1(S2) sources occurs near the G1 surface region. These electrons will be swept by corresponding D1 (D2) electric field lines and directed toward the G2 channel, forming subthreshold drain current. It is important to emphasize that, unlike in the above-threshold mode, the transversal current of subthreshold device operation is more widely spread across the $p^-$ intrinsic fin area yielding a weaker "carrier domain"-like effect.

The two different modes of DG SDS MAGFET operation are clearly reflected in the shape of the Gummel plots shown in Fig. 3, simulated for $V_{DS}$ = 3 and 5 V. Since the subthreshold region is mainly predominated by bipolar injection, the total drain current $I_{D1}+I_{D2}$ increases exponentially with $V_{GS}$ and saturates when reaching the above-threshold

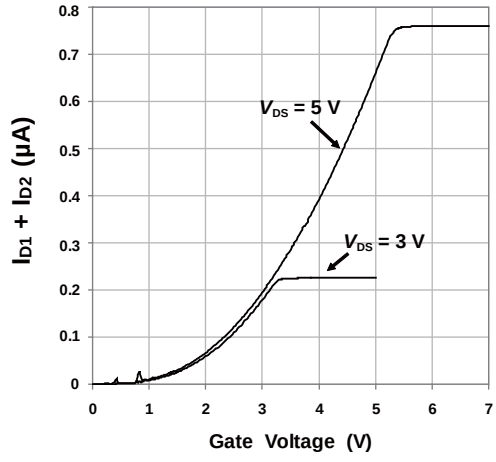


Fig. 3. Simulated Gummel plots of DG SDS MAGFET total drain currents ($I_{D1}+I_{D2}$) at $V_{DS}$ = 3 and 5 V.

region where $V_{GS} \geq V_{DS}+V_{t0}$. This can be explained as follows. Since the G1 channel is fully inverted in the above-threshold region, the location of peak electron injection forming the transversal current flow lies in the central region of the G1 channel, as observed in Fig. 2(b). In addition, since the magnitude of transverse electron injection from the G1 channel is determined only by D1(D2) electric field, the total drain current in the above-threshold region will depend only on $V_{DS}$. Consequently, being insensitive to $V_{GS}$, the total drain current shown in Fig. 3 must saturate in the above-threshold region if $V_{DS}$ = constant. For higher values of $V_{DS}$, however, a larger electron injection from G1 towards G2 will occur, yielding a higher saturation value of total drain current in the above-threshold region, as shown in Fig. 3.

### 2.3 *Magnetic behavior*

To access the device magnetic behavior, we refer to Fig. 4, which shows the directions of electron velocity $\vec{v}$ and associated Lorenz forces $F_L$ in various regions of the DG SDS MAGFET structure. These directions are based on[3]

$$F_L = q\cdot(\vec{v}\times\vec{B}_y), \tag{1}$$

where q is the electron charge, $\vec{v}$ is the electron velocity vector, and $\vec{B_y}$ is the perpendicular magnetic field vector. It is immediately clear from Fig. 4 that the ideal symmetry of the transversal electron flow appearing for $\vec{B_y}$ = 0 will be disturbed in the case of $\vec{B_y} \neq 0$, favoring the D2 side of the transversal current. This means that, depending on the magnitude of $\vec{B_y}$, some electrons injected from the S1 source will not be collected by its corresponding D2 drain via the G2 surface channel as in the case of $\vec{B_y}$ = 0. Instead, they will be collected by the D2 electrode through its associated half of the G2 channel. In turn, this will induce a difference between the two drain currents $\Delta I_D$

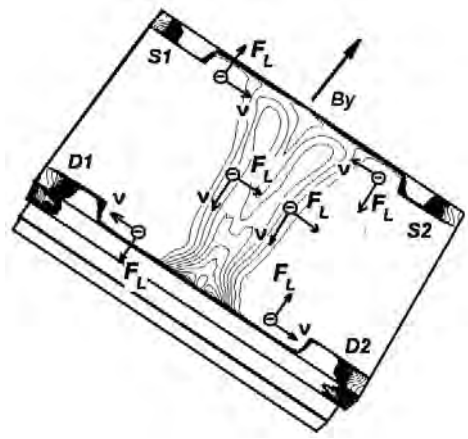


Fig. 4. Directions of the Lorenz forces $\vec{F_L}$ and the electron velocity $\vec{v}$ shown in various regions of the sensor structure.

$= I_{D2}–I_{D1} > 0$ at the device output. The higher the magnitude of $\overrightarrow{B_y}$, the larger the current difference $\Delta I_D$ will be. To satisfy the current continuity condition, the occurrence of $\Delta I_D$ is ultimately followed by a corresponding S1 (S2) source current difference $\Delta I_S = I_{S1}–I_{S2} > 0$.

Figure 4 also shows that, for a sufficiently long gate device, a non-negligible $F_L$ will affect the electron flow along the $x$-axis in the G1 and G2 channel regions. A more important factor of device sensitivity is the $F_L$ effect in the G1 channel region. Namely, as shown in Fig. 4, the direction of $F_L$ favors the formation of the G1 channel by collecting all the injected electrons from S1, while it simultaneously opposes the attraction of the S2 injected electrons by their corresponding G1 channel part. The opposing effect of $F_L$ yields a disturbed symmetry inside the G1 channel electron flow, where the number of S1 electrons forming transversal current increases while the number of S2 electrons decreases. This asymmetrical electron injection effect in the G1 channel central area, together with the shift of transversal current flow toward D2, forms a kind of positive loop with simultaneous increases in $\Delta I_D$ and $\Delta I_S$ until a new equilibrium of internal current density distribution is reached for a given $\overrightarrow{B_y}$. Note that, with respect to the vector directions in Fig. 4, an equivalent but negative current difference $\Delta I_D = \Delta I_S < 0$ will occur in the case of applying a negative magnetic field, $-\overrightarrow{B_y}$.

Our previous intuitive physical considerations can be confirmed in Fig. 5, which shows the current density distributions in the DG SDS MAGFET simulated at $V_{GS} = 5$

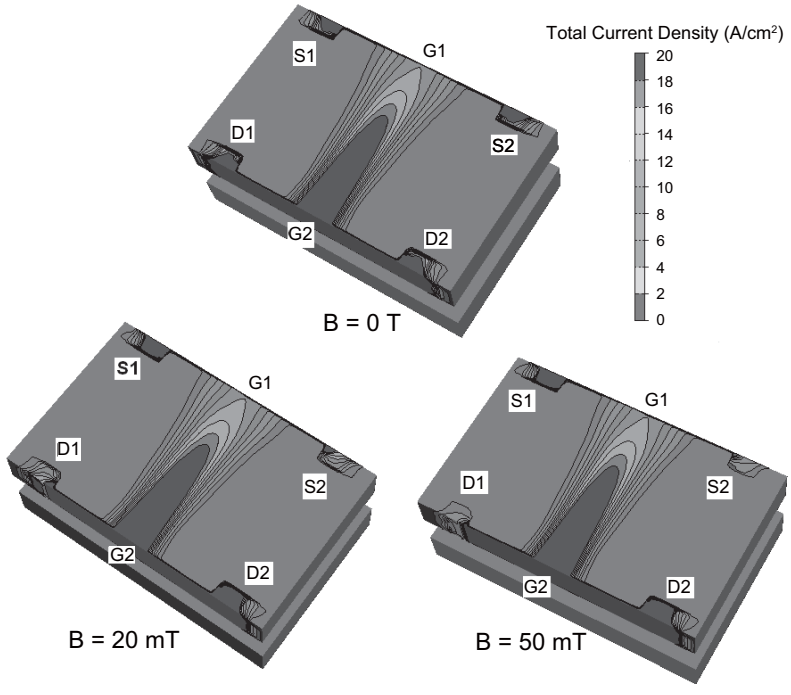


Fig. 5. Comparisons of the current density distributions simulated for $B_y$ = 0, 20, and 50 mT at $V_{GS}$ =5 V and $V_{DS}$ = 3 V.

V and $V_{DS}$ = 3 V for $B_y$ = 0, 20, and 50 mT. For $B_y$ = 0 T, the peak current densities (red areas) of Fig. 5(a) are equal in all $n^+$ diffused areas of S1, S2, D1, and D2. For $B_y$ = 20 mT, however, the red areas become notably smaller and proportionally larger in S2 and D1 and in S1 and D2, respectively, as shown in Fig. 5(b). In the case of $B_y$ = 50 mT, the red areas practically disappear in the S2 and D1 diffused regions, while they are doubled in the S1 and D2 diffused regions. The latter observation indicates that the total current in the DG SDS MAGFET for $B_y$ = 50 mT is now directed to flow only between the S1 and D2 electrodes. This reveals a potentially new application of the DG SDS MAGFET as a magnetic-controlled bidirectional cross-switch, which will be further discussed in the next subsection.

## 3. Sensitivity Simulation and Discussion

Figure 6 shows Gummel plots of the DG SDS MAGFET biased with $V_{DS1}$ = $V_{DS2}$ = 3 V, which is simulated for different $B_y$ values. Complementary effects, namely the simultaneous decrease and increase in $I_{D1}$ and $I_{D2}$ currents, respectively, with increasing $B_y$, can be observed in Fig. 6, which agree well with the physical considerations made in §2.3. More importantly, however, Fig. 6 shows that the new sensor exhibits different magnetic sensitivities in the subthreshold and above-threshold regions. Thus, a relatively small $\Delta I_D$ is obtained in the subthreshold region where $V_{GS} < V_{DS}+V_{t0}$, as shown in Fig. 6. This

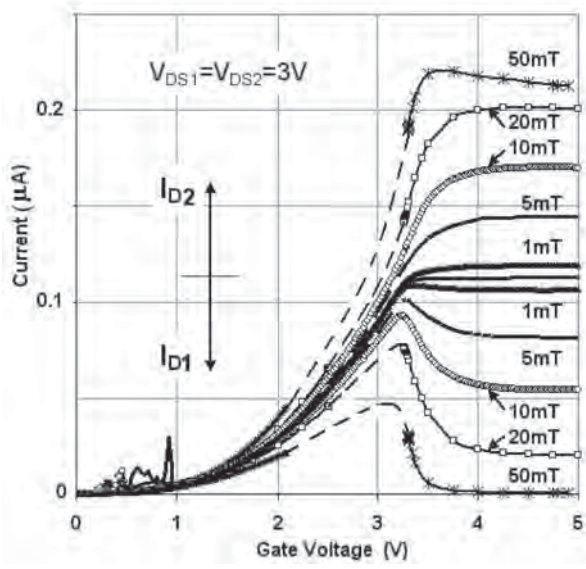


Fig. 6. Gummel plots of DG SDS MAGFET drain currents $I_{D1}$ and $I_{D2}$ simulated for various magnetic fields $B_y$ at $V_{DS1}$ = $V_{DS2}$ = 3 V. The dashed lines represent the best-fit extrapolation through noisy results due to numerical convergence problems.

can be attributed to bipolar-predominated injection from S1 and S2 resulting in a more dispersive transversal current flow with a weaker carrier domain effect, as explained in §2.2. This produces a smaller transversal current shift toward D2 for a given $B_y$, yielding a smaller drain current difference $\Delta I_D$. In contrast, in the above-threshold region defined for $V_{GS} \geq V_{DS}+V_{t0}$, the G1 channel is fully inverted. In this case, the existence of a strong carrier domain in transversal current flow as well as that of a positive loop in the G1 channel (explained in §2.3) is observed in simulations yielding a much larger current difference $\Delta I_D$ for the same $B_y$, as shown in Fig. 6.

In the case of very low magnetic fields (< 1 mT), the absolute current difference $\Delta I_D$ obtained at high sensitivity in the above-threshold region can sometimes be insufficient for extracting a useful sensor signal from a high-noise floor. In this case, the absolute value of $\Delta I_D$ at low $B_y$ could be enhanced using higher $V_{DS}$ and $V_{GS}$ voltages in the above-threshold region, as shown in Fig. 7. The signal-to-noise ratio of the sensor can be improved at low magnetic fields, but at the expense of device power dissipation.

Figure 8 shows the variations in $I_{D2}$, $I_{D1}$, and $\Delta I_D$ with magnetic field $B_y$ extracted at $V_{GS}$ = 5 V from the results in Fig. 5. The differential current relative magnetic sensitivity $S_R$ of the DG SDS MAGFET is defined as

$$S_R = (I_{D1}+I_{D2})^{-1} \cdot \frac{\partial(\Delta I_D)}{\partial B_y}\bigg|_{B_y=0}. \quad (2)$$

From eq. (2) and using the results in Fig. 7, it is found that $S_R$ varies from $S_{Rmax}$ = 56 T$^{-1}$ to $S_{Rmin}$ = 18 T$^{-1}$ in the $B_y$ range from 1 to 30 mT, respectively. Although predicted from simulation, it is still 40 to 50 times higher than the sensitivity found in conventional MAGFETs,[6–8] indicating the good potential of the new magnetic sensor design. It is also important to emphasize that the sensitivity of the DG SDS MAGFET depends on the particular device geometry and chosen SOI technology parameters. The optimization of

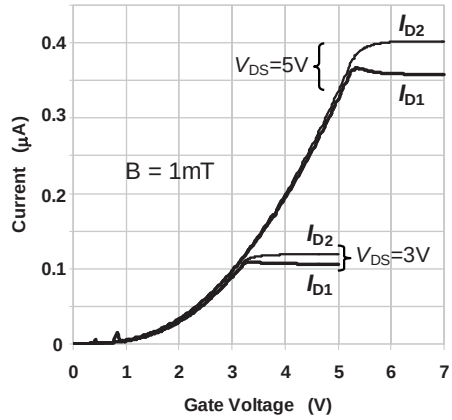


Fig. 7. Method of increasing the absolute drain current difference ($I_{D1}$–$I_{D2}$) of DG SDS MAGFET at low magnetic field $B_y$.

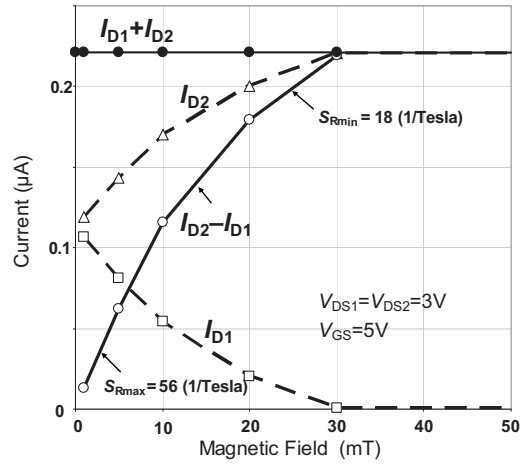


Fig. 8. Variations in drain currents $I_{D2}$ and $I_{D1}$ and their difference ($I_{D1}$–$I_{D2}$) versus the magnetic fields $B_y$ extracted for $V_{GS}$ = 5 V and $V_{DS1}$ = $V_{DS2}$ = 3 V.

the sensor structure with respect to maximizing $S_R$ and other electrical characteristics as well as the evaluation of experimental devices will be the subject of further research.

Finally, the results in Fig. 7 show that $S_R$ abruptly approaches zero for $B_y \geq 30$ mT since the ratio $I_{D2}/I_{D1}$ becomes larger than $10^4$ at higher magnetic fields. This means that, when the external field $B_y$ increases above 30÷50 mT, the S1 and D2 electrodes practically take up the total conduction current through the device, whereas the S2 and D1 electrodes acquire negligible input/output currents. This effect is clearly seen in the current density distributions shown in Fig. 5(c), where no red areas exist in the S2(D1) $n^+$ diffusion regions for $B_y$ = 50 mT. This also means that, by applying an external time-varying pulsed magnetic field $\pm\vec{B}_y(t)$ with $B_y$ > (30÷50) mT, the total current through the DG SDS MAGFET can be directed to flow either through the S1 and D2 electrodes or via the S2 and D1 electrodes depending on whether a positive or negative $B_y$ is applied, respectively. This important conclusion obtained from device simulations implies that the DG SDS MAGFET can operate not only as a low-field magnetic sensor, but also as a bidirectional electric cross-switch controlled by an external pulsed magnetic field. In due course, it is worth considering the idea of integrating a DG SDS MAGFET and a micromachined inductive metal coil placed on top of a sensor device, thus forming the matrices of magnetically controlled cross-switches in FD SOI technology.

## 4. Conclusions

We described the design and operation of a DG SDS MAGFET compatible with fully depleted (FD) thin-film silicon-on-isolator (SOI) technology. Using a realistic 3D device numerical simulation, we showed that the relative magnetic sensitivity of the DG SDS MAGFET can reach 58 $T^{-1}$ in the mT range of magnetic fields. Although obtained from device simulations, the predicted sensitivity was more then two orders of magnitude higher than that found in conventional MAGFETs fabricated using FD SOI technology. We also revealed that the DG SDS MAGFET can operate as a bidirectional cross-switch controlled by pulsed magnetic fields with a minimum amplitude of 30 mT. Further work is required to optimize device design and to evaluate predicted magnetic sensor behavior with experimental results.

## Acknowledgement

This work was supported by the Serbian Ministry of Science and Technological Development.

## References

1 H. P. Baltes and R. S. Popovic: Proc. IEEE **74** (1986) 1107.
2 J. E. Lenz: Proc. IEEE **78** (1990) 973.
3 S. M. Sze (Ed.): Semiconductor Sensor (Wily-Interscience Publication, New York, 2000).
4 D. Flandre, S. Adriaensen, A. Afzalian, J. Laconte, D. Levacq, C. Renaux, L. Vancaillie, J.-P. Raskin, L. Demeûs, P. Delatte, V. Dessard and G. Picun: IEEE Sensors **2** (2002) 1407.
5 B. Gentinne, J.-P. Eggermont, D. Flandre and J.-P. Colinge: Mater. Sci. Eng., B **46** (1997) 1.
6 L. Demeûs, V. Dessard, A. Viviani, S. Adriaensen and D. Flandre: IEEE Trans. Ind. Electron. **48** (2001) 272.
7 P. Losantos, C. Cane, D. Flandre and J.-P. Eggermont: Sens. Actuators, A **67** (1998) 96.
8 G. Picún and D. Flandre: Electrochemical Society Proc. (Washington DC), 2001–3 (2001) p. 289.
9 SILVACO User's Manual (SILVACO International Inc., 2000).
10 D. Hisamoto, T. Kaga and E. Takeda: IEEE Trans. Electron. Devices **38** (1991) 1419.
11 J. Lau, C. T. Nguyen, P. K. Ko and P. C. H. Chan: IEEE Trans. Electron. Devices **41** (1996) 1851.